Aeroacoustics of in-flight propeller-wing in pusher configuration

Deepak C Akiwate *, Riul Jung†
Acoustics Research Centre, University of Salford, 43 Crescent, Salford, Manchester, M5 4WT, United Kingdom

Paruchuri Chaitanya‡, Phillip Joseph§, A B. Parry¶
Institute of Sound and Vibration Research, University of Southampton, Southampton, UK, SO17 1BJ

David Angland ‖
University of Southampton, Burgess Road, Southampton SO16 7QF UK

In this study, we investigate the noise produced by a propeller installed in a pusher configuration in close proximity to a wing. Experiments are conducted in a state-of-the-art anechoic wind tunnel to observe the impact of both static and in-flight conditions on overall noise generation. We found that as the separation distance increases, the interaction between the propeller and wing diminishes, causing the overall noise to approach levels similar to those of the rotor alone. A comprehensive comparison of predictions and measured results across various separation distances aids in understanding dominant noise mechanisms over a range of propeller and wing separations. At low separation distances, the potential field is the dominant mechanism of noise generation, while at higher separations, wake interaction is found to be the dominant source. This, in turn, facilitates understanding of noise generation from installed propellers and enables the design of low-noise configurations and the establishment of noise control strategies for installed propellers.

I. Introduction

In recent years, there has been a notable increase in the adoption of propeller-based architectures, such as regional aircraft, Urban Air Mobility (UAM), and propeller drones, driven by the emergence of electric and distributed propulsion systems [1]. These systems, known for their lightweight nature, offer 10-20% higher performance compared to conventional turbofan engines at moderate flight speeds [2, 3]. According to a report, the advanced air mobility market in the United States alone is projected to reach a substantial annual value of $115 billion USD by 2035 [4]. However, a significant concern associated with propeller-driven aircraft is their noise level, attributed to steady loading and unsteady aerodynamic loading caused by various interaction mechanisms related to the propeller installation [3, 5, 6].

Understanding the various noise sources linked to propeller architectures is crucial. Notably, the propeller-wing configuration, with the propeller mounted in a pusher configuration, is a key feature of advanced propulsion systems. Akiwate et al. [7] have discussed the various noise sources associated with propellers installed in a puller configuration [8]. It's important to note that the noise characteristics of an installed propeller in operation differ significantly from those of an isolated propeller [9–12]. The noise radiation from an isolated propeller with subsonic tip speed is well understood, following the pioneering work of Gutin [13]. Over the last few decades, the tonal interaction noise of contra-rotating propellers has been extensively discussed, and theoretical formulations for noise radiation from contra-rotating propellers are well developed and validated [3, 5, 14–19].

The current study focuses on an experimental campaign of installed propeller noise in both static and in-flight conditions, comparing the results with available analytical prediction schemes. This study is conducted in the state-of-the-art anechoic wind tunnel facility at the Boldrewood Innovation Campus, University of Southampton. During experiments, various parameters are considered, including the separation distance between the propeller and wing, in-flight and static conditions, and wing incidence. These experimental results provide deeper insights into

*University Fellow, University of Salford, member AIAA, d.c.akiwate@salford.ac.uk.
†KTP Associate, University of Salford, R.Jung@salford.ac.uk.
‡RAEng Research fellow and Associate Professor, ISVR, ccp1m17@soton.ac.uk.
§Professor, ISVR, Senior member AIAA, pfj@soton.ac.uk.
¶Consultant, ISVR, Senior member AIAA, A.Parry@soton.ac.uk.
‖Associate Professor, Department of Aeronautics and Astronautics, d.angland@soton.ac.uk.

noise generation mechanisms, including both tonal and broadband components. Comparing predicted results with measurements will help understand dominant noise generation mechanisms and establish effective control strategies.

II. Experimental set-up and procedure

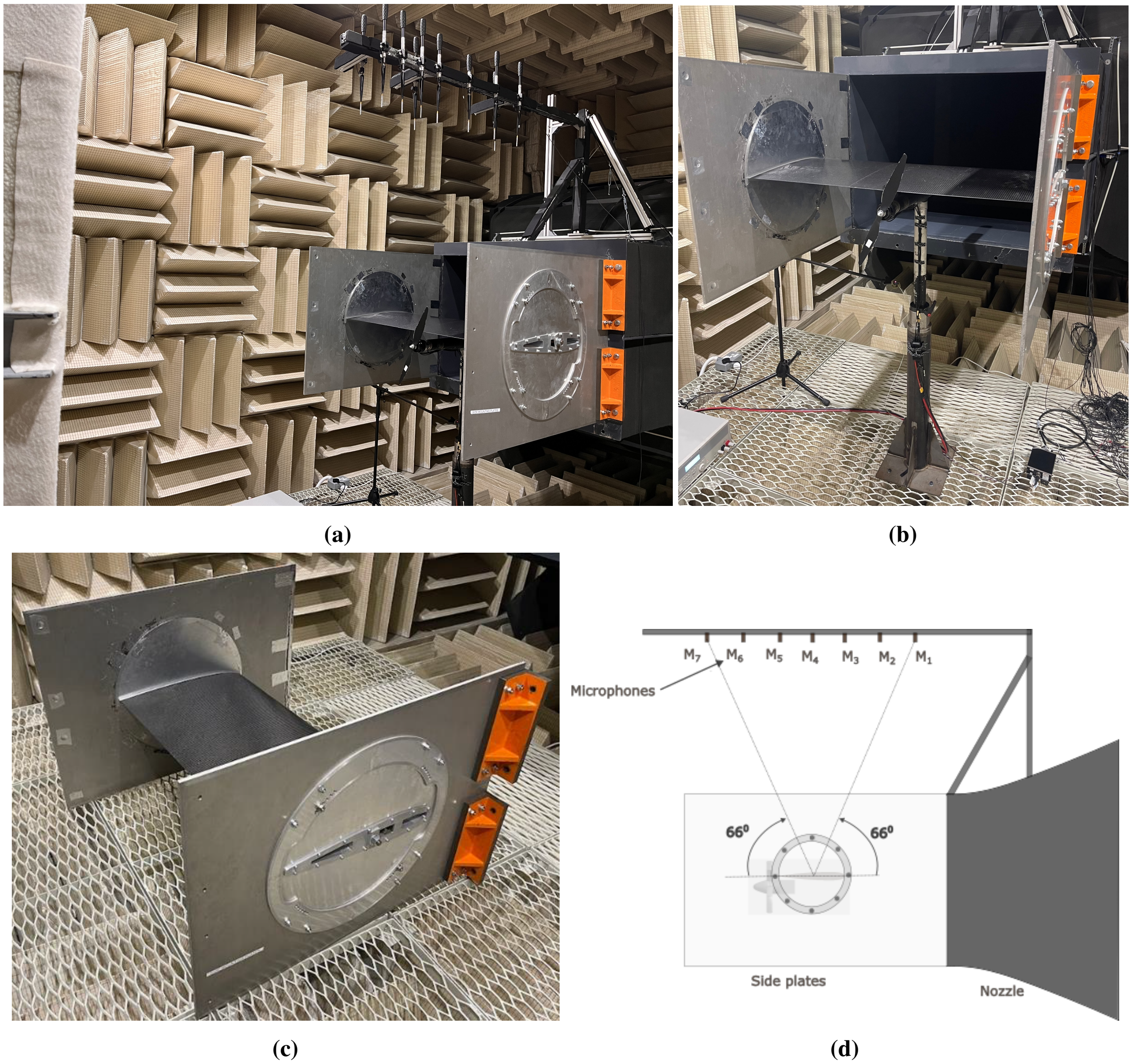

Fig. 1 (a) photograph of experimental rig inside the anechoic wind tunnel (b) close view of the prop-wing configuration and mountings (c) photograph of wing mounted on side plate (d) schematic of microphone array

A. Propeller rig

The experimental investigation was conducted on the 16x5.5 APC propeller. The rig consisted of a rotor powered by a U7-V2.0 KV280 motor from T-Motor, mounted on a MINI45 ATI 6-axis load cell. An Electronic Speed Controller (FLAME 80A 12S V2.0 ESC) was used to control the motor speed to produce the required thrust by the propeller. The precise rotational speed of the propellers was measured using an ICP Laser Tachometer sensor. The complete propeller setup with load cell and motor was mounted to the hand-adjustable and lockable stand, as seen in Fig. 1b. The separation distance between the propeller and wing was varied by moving the propeller forward and backward using an adjustable stand while the wing was fixed in position by side plates. Due to the relatively low maximum torque (1.209 N-m) of the rig, the experiments were conducted at a maximum flow speed of 25m/s. At this maximum speed, we were still able to achieve 10N of thrust. Therefore, all our experiments were limited to a thrust of 10N.

B. Wing geometry

For the experiments, we utilized a symmetrical NACA0012 airfoil made of carbon fiber. The airfoil had a chord length of 0.5m and a span of 1m. It was affixed between two circular aluminum side plates (10mm thickness, 260mm radius). The construction involved a thin carbon fiber shell enveloping a single rectangular aluminum spar at the maximum thickness point. Despite the airfoil featuring pressure tapings along its centerline, they remained unconnected and unused in this experiment.

To install the aerofoil in the wind tunnel nozzle, we utilized a pair of 10mm thick aluminum side plates. These plates were connected to the nozzle flange through a set of 4 stainless steel L brackets bolted to the end of each plate (2 on each side, as shown in orange color in Fig. 1c). The plates were flush-mounted with the interior wall of the nozzle. Each side plate featured a large circular recess at its center, allowing for the flush mounting of the aerofoil and its smaller circular side plates. To adjust the aerofoil's angle of incidence, we rotated it within its circular recess and secured it at pre-drilled 5-degree intervals, up to a maximum angle of 20 degrees. It's crucial to note that the aerofoil could only be operated at a maximum angle of 5 degrees of incidence. Beyond this point, the jet from the nozzle would miss the collector, as it was directed downward at higher angles of incidence. Therefore, we restricted our measurements to the 0 and 5 degrees of angle of incidence.

C. Microphone array and far-field measurements

A linear array of 7 microphones was chosen for the tests. This array allowed us to measure the broadband and tonal band noise and calculate the overall sound power around the mid-chord of the aerofoil. GRAS 46BE high-performance ¼" free-field microphones were employed across this array, with 7 microphones distributed along an aluminum cantilever beam mounted to the roof of the wind tunnel nozzle (refer to Fig. 1d). This linear microphone array covered the polar angle of aperture from 66 degrees to 114 degrees. Microphone 5 was positioned in line with the trailing edge of the aerofoil. The distance between microphone 5 and the trailing edge of the wing at zero degrees of angle of incidence was 1.078m.

Acoustic pressure levels were recorded at a fixed 10N of thrust across varying rotor aerofoil separation distances (Z/D) from 0 to 1. The conversion of sound pressure measurements to sound power was accomplished using equation 1.

$$S_w(\omega) = \sum_{i=1}^{i=N-1} \frac{[S_{PP}(\omega, \theta_i) + S_{PP}(\omega, \theta_{i+1})]\, \pi R^2 \sin(\theta) \Delta\theta_i}{\rho c} \tag{1}$$

In this equation, $S_\omega(\omega)$ represents the spectral density of sound power radiated over the range of polar angles. $S_{PP}(\omega, \theta_i)$ denotes the acoustic pressure (Power Spectral Density) measured from a microphone in the array at polar angle θ_i with respect to the rotor axis. The variables R, θ, $\Delta\theta_i$, ρ, and c are defined as follows: R is the radius of the microphone array, θ is the polar angle of the microphone position with respect to the rotor axis, $\Delta\theta_i$ is the angle between two adjacent microphones in the array, ρ is the density of the ambient air, and c is the speed of sound. Sound Power Level spectra was calculated from spectral density by $\mathrm{PWL}(\omega) = 10\log_{10}(S_w(\omega)/W_{ref})$. The Overall Sound Power Level (OAPWL) is calculated over a frequency range from 90Hz to 12kHz using $\mathrm{OAPWL} = \frac{\int_{90}^{12500}(S_\omega)}{\mathrm{W_{ref}}}$. Here, $\mathrm{W_{ref}} = 10^{-12}$ W is the reference acoustic power.

III. Analytical predictions

The noise generation mechanism of the rotor operating close to the other structures such as a wing is quite different from a single propeller in an uninstalled condition [7, 9–12, 20–22]. When a rotor is closely spaced to a wing, such as a prop-wing configuration in UAM, drones or regional aircraft, acoustic and aerodynamic interaction occurs between the rotor and the wing. In the current study we are focusing on such such prop-wing configuration with a wing located at upstream of the rotor. The noise generation mechanisms of the rotor in uninstalled conditions are already described in the previous literature [3, 5, 23]. However, this section provides a quick summary of the prediction schemes used in the current study. We utilise analytical or semi-analytical prediction schemes for each type of source mechanism involved, including rotor in both uninstalled and installed conditions [7]. Most noise sources have tonal and broadband components.

1. Tonal noise

The mean square tonal sound pressure $\overline{P_{mn}^2}$ at the discrete harmonic of combination of m^{th} and n^{th} indices is expressed in terms of the geometric and working parameters as

$$\overline{P_{mn}^2}\left(r_0,\theta,\omega\right)=2\left(\frac{BR_t}{4\pi r_o\left(1-M_x cos\theta\right)}\right)^2\times\left|\ \mathrm{I}\ \right|^2 \tag{2}$$

Here, B, R_t, and r_o are the blade number, propeller tip radius, and observer distance, respectively. The term I is spanwise integral which consists of the source term, radiation term, and the source non-compactness along the chord. This integral varies for each type of source and it can be expressed in general form as

$$\overline{P_{mn}^2}\left(r_0,\theta,\omega\right)=2\left(\frac{BR_t}{4\pi r_o\left(1-M_x cos\theta\right)}\right)^2\ \left\{|\mathrm{I}_{\mathrm{RA}}|^2+\ |\mathrm{I}_{\mathrm{VSCW}}|^2+|\mathrm{I}_{\mathrm{TVRT}}|^2+|\mathrm{I}_{\mathrm{FPOT}}|^2+|\mathrm{I}_{\mathrm{RPOT}}|^2\ \right\} \tag{3}$$

In general, the integral I is of type

$$\mathrm{I}=\int_{r_h}^{R_t} S\left(r\right)J_\nu\left(\overline{k}_{mn}R_t sin\theta z\right)dz \tag{4}$$

where, r_h is the hub radius, $z = rR_t$ is non-dimensional radius, J_ν is the Bessel function of order ν which is related to front rotor blade number (B_F) and rear wing blade number (B_R) as $\nu = mB_F - nB_R$. Here m and n are the indices for the front rotor and rear wing, respectively. I_{RA}, $\mathrm{I}_{\mathrm{VSCW}}$, $\mathrm{I}_{\mathrm{TVRT}}$, $\mathrm{I}_{\mathrm{FPOT}}$, and $\mathrm{I}_{\mathrm{RPOT}}$ are the integrals for rotor-alone, viscous-wake interaction, tip-vortex, forward potential, and rearward potential, respectively. The $\overline{k}_{mn} = \omega_{mn}/[c_0(1 - M_x cos\theta)]$ is the discrete wave number at respective frequencies. A special case where index $n = 0$ represents a case of rotor-alone under investigation. This represents the stationary loading on the rotor blades. One of the important terms in integral is source $S(r)$ which depends on the type of source mechanism under consideration.

2. Broadband noise

Broadband self-noise of the rotor is produced by the interaction of the boundary layer with its trailing edge while the interaction broadband noise is generated due to the impingement of the turbulent wakes of the front wing on the leading edge of the rear rotor. The prediction scheme used in the current study is based on the semi-empirical formulation of Blandeu [6] which takes account of source non-compactness along the chord and makes use of strip theory to account for spanwise variation of geometric and aerodynamic parameters. For self-noise, isolated flat plate response by Amiet [24, 25] is used with correction by Roger and Moreau [26] to consider the effect of skewed gusts, and the surface pressure spectrum at the trailing edge is computed by the model proposed by Rozenberg [27]. The panel method code XFOIL [28] was used to estimate the boundary layer parameters at the trailing edge of propeller blade and wing, which serves as input to the surface pressure spectrum model. In the case of interaction noise, turbulent wake parameters are estimated from the mean wake parameters and the unsteady response of the rear blades is computed from the method described by Amiet [29, 30]. The broadband sound pressure level from the pressure spectral density SS_{pp} for respective broadband sources is estimated by the following expression.

$$\mathrm{SPL}_{\mathrm{BB}}\left(r_0,\theta,\omega\right)=10\log_{10}\left(\frac{2\ bw\ SS_{pp}\ \left(r_0,\theta,\omega\right)}{P_{ref}^2}\right) \tag{5}$$

Here, bw is the bandwidth for the $1/3^{rd}$ octave band. The pressure spectral density for the trailing edge self-noise SS_{pp}^{TE} and wake interaction noise SS_{pp}^{RWIB} is given by

$$SS_{pp}^{TE}\left(r_0,\theta,\omega\right)=\frac{B}{2\pi}\left(\frac{k_0 b_1}{r_0\left(1-M_x cos\theta\right)}\right)^2\Delta r\sum_{l=-\infty}^{\infty}D_l\left(\theta,\alpha,\omega\right)|\mathcal{L}^{TE}\left(k_r=0,K_{X,l},\kappa_l\right)|^2 S_{qq}(0,K_{X,l}) \tag{6}$$

$$SS_{pp}^{RWIB}\left(r_0,\theta,\omega\right)=\frac{1}{4}\left(\frac{B_F B_R\times\rho_0 k_0 b_2}{r_0\left(1-M_x cos\theta\right)}\right)^2 U_{r2}\Delta r\sum_{q=-\infty}^{\infty}\sum_{m=-\infty}^{\infty}\sum_{n=-\infty}^{\infty}D_{ml}\left(\theta,\alpha_2,\omega\right)\Phi_{\omega\omega}\left(k_r=0,K_{X,qmn},K_{Y,qmn}\right)|\mathcal{L}^{LE}\left(k_r=0,K_{X,qmn},\kappa_{qmn}\right)|^2 \tag{7}$$

Here, b, Δr, q, U_r, k_r are the half chord length, strip width, turbulence azimuthal mode order, sectional velocity, and span-wise wave number, respectively. Subscripts 1 and 2 are used to denote the quantity or parameter related to the respective wing or rotor. D_l and D_{ml} are the radiation terms for respective sources while $\mathcal{L}^{TE}$ and $\mathcal{L}^{LE}$ are the unsteady loading term due to trailing edge and leading edge, respectively. $\Phi_{\omega\omega}$ is the wave number spectrum of turbulent upwash velocity and S_{qq} is the wavenumber spectral density of the surface pressure cross-spectrum. A more detailed explanation and estimation of the above terms is given in PhD thesis [6].

IV. Results

In this section, we will look into the acoustic measurements obtained using the linear microphone array discussed in the previous section. In order to comprehend the impact of wind speed and installation effects, we conducted a series of measurements for the propeller alone, the propeller with side plates, and the propeller-wing with side plates at various flow speeds and separation distances between the propeller and wing. Additionally, we explored the influence of the wing angle of incidence on the overall noise of the propeller-wing configuration. In the following subsection, we will analyse the effects of these individual parameters on the overall noise. Further, we have compared the noise levels from the pusher (propeller downstream of wing) configuration with those of puller (propeller upstream of wing) for the same thrust and separation distance between propeller and wing.

Prior to conducting any sound measurements, all microphones were calibrated with the pistonphone, and the load cell and tachometer were calibrated and verified using propeller performance data.

A. Rotor alone

At first, we performed measurements of the propeller's performance at various speeds and compared them with the baseline data provided by the manufacturer. Next, a series of baselines were established to observe background noise from the wind tunnel and the effects of adding certain apparatus into the anechoic chamber.

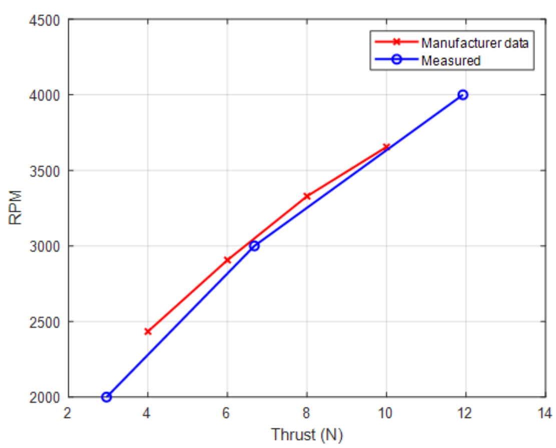

(a) rotor alone performance comparison without flow

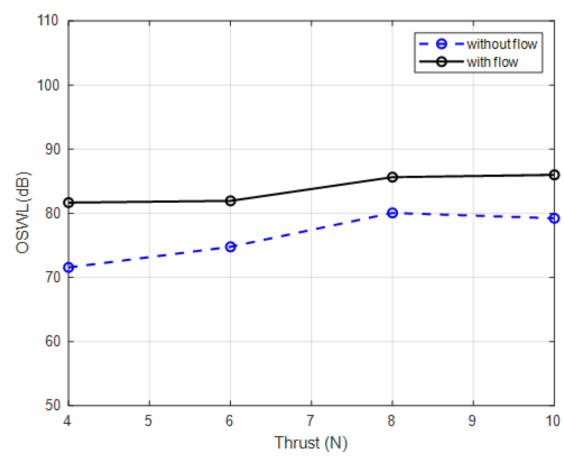

(b) rotor alone noise with flow and without flow

Fig. 2 (a) comparison of measured propeller performance with manufacturer data (b) rotor alone OSWL with flow at U=15m/s and without flow

In the initial scenario, the wind tunnel ran without any propeller-wing or side plate inside the chamber (except for the microphone array), and background noise was noted to ensure it didn't affect the measurements. This was carried out at four different flow speeds: 0, 15, 20, and 25 m/s. Following that, the rotor and stand were mounted to the mesh floor. At four different fixed thrusts (4, 6, 8, 10N), baselines were recorded for the stationary rotor (U=0) and in-flight rotor (U=15m/s). All experiments were conducted using a 16x5.5 APC propeller.

Figure 2a displays the comparison of measured and manufacturer performance data over a range of thrust at a no-flow condition. It is observable that the speed-versus-thrust curve closely aligns with the given data, indirectly confirming the calibration of the tachometer and load cell used to measure speed and thrust produced by the propeller.

As a first step, we examined the rotor-alone Overall Sound Power Level (OSWL), which integrates over frequency and space, to observe the variation in propeller noise over the thrust range for both with and without flow conditions.

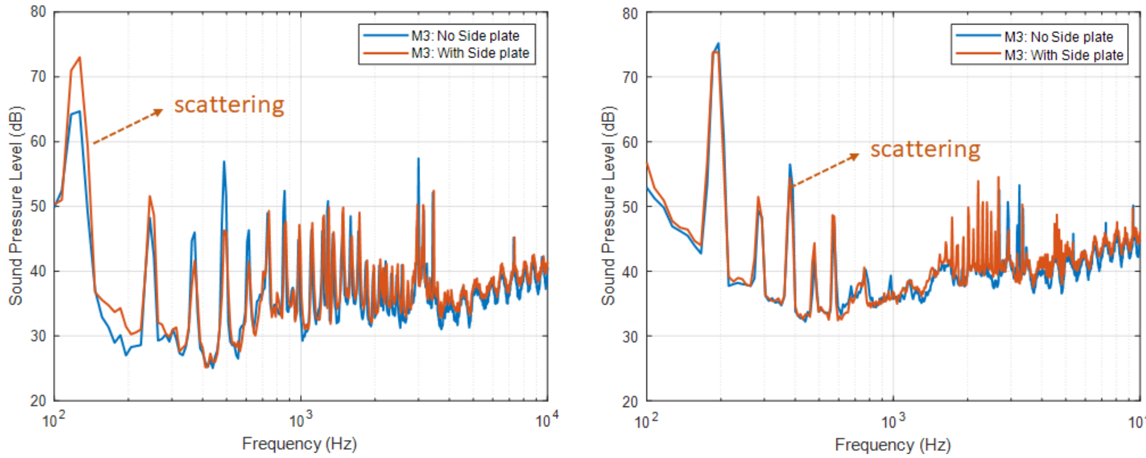

(a) rotor alone without flow **(b) rotor alone with flow at U=15m/s**

Fig. 3 Rotor alone SPL at microphone location 3 with and without side plates at 10N thrust

For this study, a flow condition of U=15m/s was chosen. With flow, to produce the same thrust as that of the no-flow condition, the propeller had to run at a much higher rpm compared to the no-flow condition. Results showed that, as expected, with flow, the overall noise level of the propeller increased due to both an increase in tonal and broadband noise source strengths.

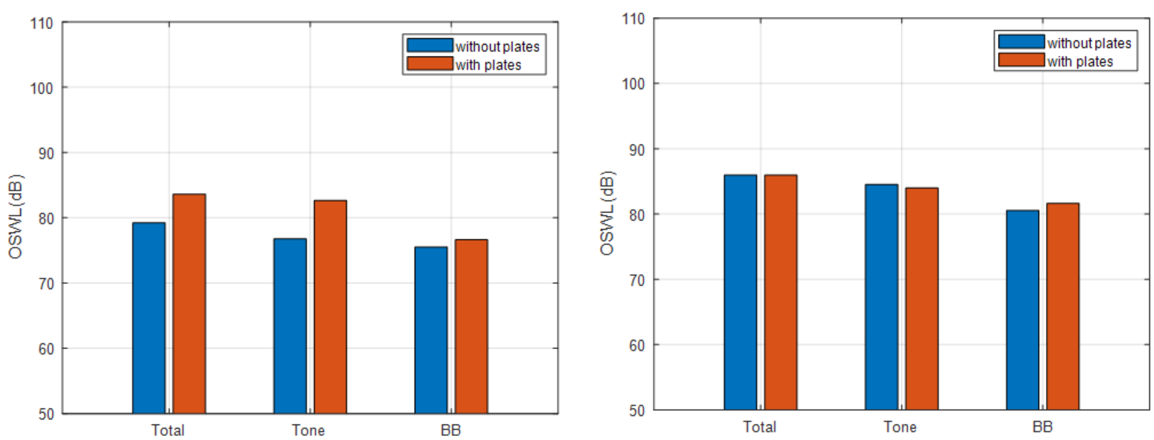

(a) rotor alone without flow **(b) rotor alone with flow at U=15m/s**

Fig. 4 Rotor alone OSWL with and without side plates at 10N thrust

Further, the entire propeller-wing configuration had to be tested together with the wing-mounting side plates. These mounting plates might add considerable noise to the overall measurements. Therefore, we examined the effect of the side plates on the noise spectrum from the propeller at microphone location 3 and plotted it in Fig. 3. From the spectrum plot, it can be seen that for the no-flow case (Fig. 3a), the SPL spectra were affected by the acoustic scattering due to plates, especially at the fundamental BPF where SPL was significantly amplified. In contrast, the SPL spectra were less affected in the presence of flow, as shown in Fig. 3b. This indicates that flow effects dominate over plate scattering.

Further details on how this scattering affects overall noise are shown in Fig. 4. It can be observed that scattering from the plate has amplified overall noise without flow (Fig. 4a). The increase in overall noise is predominant in its tonal component, while broadband noise remains almost the same (see Fig. 4a). However, with the flow, the overall noise levels with and without the plate remain almost the same. This could be due to the flow effect and refraction, which led to a slight reduction in tonal noise and an increase in broadband noise compared to the without-plate case. Therefore, overall noise with the plate for a flow case remains the same. The increase in tonal noise without flow due to plate scattering needs to be assessed carefully while measuring the overall noise from the complete propeller-wing configuration.

B. Wing alone

To assess the impact of wing-alone noise on the overall noise generated by the propeller-wing configuration, our initial focus was on examining wing-alone noise across a range of flow speeds. This involved removing the propeller and mounting stand, then affixing the wing to side plates and attaching it to the wind tunnel nozzle flange using L brackets, as illustrated in Fig.1c. Subsequently, we conducted measurements of the overall noise for flow speeds ranging from 10m/s to 25m/s, considering the airfoil at zero degrees ($\alpha = 0^0$) and at five degrees ($\alpha = 5^0$) of angle of incidence, as depicted in Fig. 5.

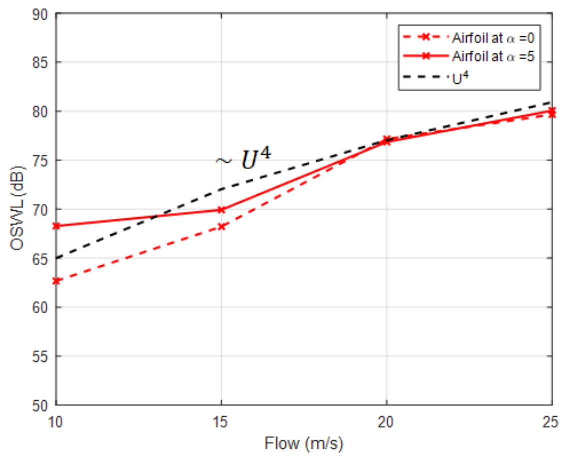

Fig. 5 Overall wing alone noise at different flow speeds.

Upon analysis, we observed that beyond U=15m/s, the overall noise from the wing remained consistent in both cases. This noise emanates from two primary sources: wing trailing edge noise, attributed to the scattering of the boundary layer, and wing leading edge noise, resulting from the interaction of incoming flow with the wing's leading edge. Notably, one of the predominant contributors to noise is the wing's trailing edge, which is primarily influenced by the thickness of the boundary layer at the trailing edge. At lower speeds and higher angles of incidence, the boundary layer thickness tends to be thicker, leading to elevated broadband noise—a trend that aligns with our current measurements.

However, at higher flow speeds, the boundary layer thickness at the trailing edge is relatively smaller, exerting a lesser impact on the overall noise. It should be noted that the broadband noise is observed to scale approximately as U^4 to the flow velocity, which is in line with expectations for broadband noise.

C. Propeller and wing

In this section we will look at the overall noise generated by the propeller-wing in pusher configuration. We looked at the two different cases of propeller-wing with wing being at angle of incidence of $\alpha = 0^0$ and $\alpha = 5^0$. The total overall noise has been compared with rotor-alone noise to evaluate the interaction noise. We also look at the effect of flow on overall noise. For current study we have performed all propeller-wing measurements at flow speed of U=15m/s and propeller thrust of 10N. Furthermore, this section also provides a comparison of noise levels with the puller (propeller upstream of wing) configuration for the same propeller and wing separation distance and thrust requirement.

1. Wing at incidence $\alpha = 0^0$ and $\alpha = 5^0$

Now, we investigate into an examination of the overall noise produced by the propeller-wing in a pusher configuration with the wing set at an angle of incidence, $\alpha = 0^0$. Fig.6 illustrates the overall noise levels, considering both scenarios with and without airflow, across a spectrum of normalized separation distances between the propeller and the wing. The separation distance (Z), measured from the propeller's hub to the wing's mid-chord location, is normalized by the propeller diameter (D). This standardization ensures a consistent basis for comparison.

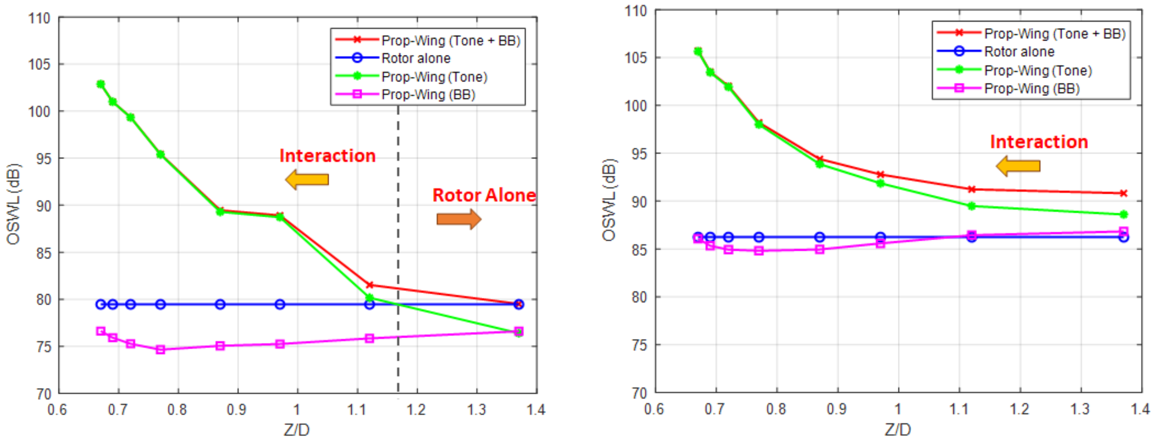

(a) Propeller wing noise with no flow **(b) Propeller wing noise with flow at U=15m/s**

Fig. 6 Propeller wing noise and its comparison with rotor alone noise at 10N thrust and at wing incidence $\alpha = 0^0$

In Fig.6a, a comparative analysis is presented, showcasing the measured overall noise alongside its tonal and broadband components in relation to the rotor-alone scenario under no-flow conditions. The results indicate a consistent trend: as the separation distance between the propeller and wing increases, the overall noise diminishes, aiming to approach the noise level produced by the rotor-alone configuration. This reduction is attributed to the decreased interaction between the propeller and wing, leading to a decline in unsteady loading on both the wing and propeller. Consequently, at significantly greater separation distances, the overall noise is predominantly governed by the rotor-alone noise.

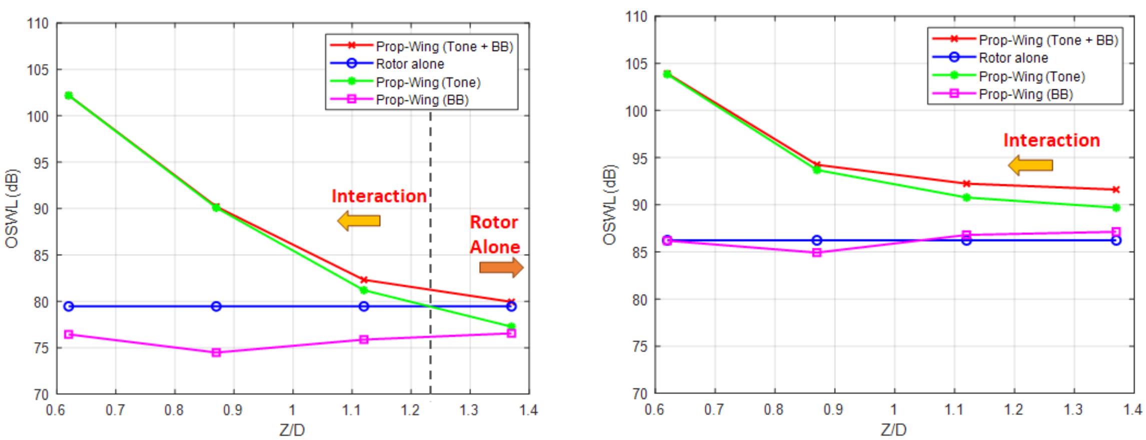

(a) Propeller wing noise with no flow **(b) Propeller wing noise with flow at U=15m/s**

Fig. 7 Propeller wing noise and its comparison with rotor alone noise at 10N thrust and at wing incidence $\alpha = 5^0$

Transitioning to Fig.6b, the focus shifts to similar measurements of the propeller-wing configuration under the influence of a flow speed of U=15m/s. As anticipated, the overall noise is notably higher in the presence of airflow (in-flight) compared to the static (no-flow) condition. This elevation in noise levels can be attributed to a substantial increase in source strengths of interaction and rotor-alone noise.

In general, the source strength of unsteady interaction acoustic noise sources increases with an increase in sectional velocity. In presence of flow, to produce the same thrust, the propeller rotates at a higher speed compared to the no-flow case, leading to higher sectional velocities and thus higher acoustic source strengths. We have observed that the interaction noise source consistently dominates over a range of separation distances considered for this study, which was not the case under no-flow conditions. This suggests that even the presence of a small flow will alter the dominant noise source mechanism for the propeller-wing configuration, and the noise may be dominated by the interaction noise sources even at higher separation distance. However, changes in propeller blade number, tip speed, and thrust requirements may alter this balance.

Figure 7 shows similar measured results to those of the previous section, but with reduced separation distance points and the wing at an incidence of $\alpha = 5^0$. We have observed similar trends to those with no wing incidence; however, overall noise (including individual noise sources) is slightly higher. This suggests that an increase in wing incidence tends to increase the unsteady interaction with the rotor. Due to constraints on wing incidence, we have restricted our study to $\alpha = 5^0$. In the near future, we will explore the effect of higher wing incidence on interaction noise sources.

2. Comparison with propeller upstream (puller)

To assess the comparative noise levels between puller and pusher configurations, this section focuses on comparing noise levels from both configurations at the same separation distance between the propeller and wing and thrust requirement. To do this, we performed noise measurements at a range of separation distances. However, the upstream propeller separation distance was limited to $Z/D = 0.87$ because the propeller was close to the nozzle of the wind tunnel. Figure 8a shows a comparison of overall noise levels for pusher and puller configurations at 10N thrust. It was observed that the puller configuration follows the same trend as the pusher configuration, but the noise level with the pusher configuration is consistently higher (approximately 5dB) than the puller configuration over the entire range of separation distances. Additionally, it is noteworthy that even though the propeller was running at a slightly higher RPM for the puller configuration (see Fig. 8b), the overall noise for the puller configuration was found to be lower. One reason for the pusher configuration being noisier is that the propeller operates in the wakes of the wing and produces higher unsteady noise. This suggests that the puller configuration will be acoustically advantageous compared to the pusher configuration for the same propeller thrust and separation distance between the propeller and wing. However, their detailed aerodynamic performance needs to be assessed for the particular aircraft architecture and design requirements. We will be able to see the individual dominant mechanisms for the pusher configuration in the next section.

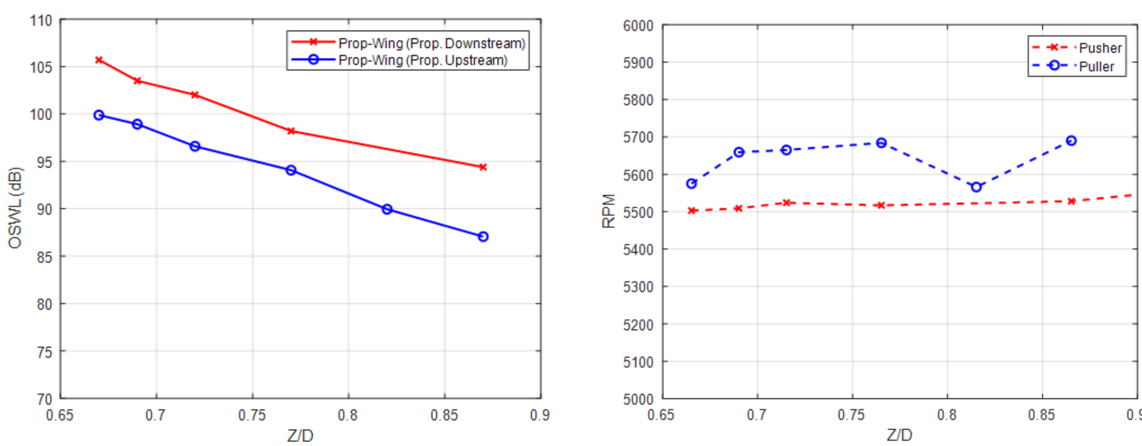

(a) Overall noise levels of pusher vs puller **(b) Propeller RPM with flow at U = 15 m/s**

Fig. 8 Comparison of pusher and puller configurations at U=15m/s and 10N thrust.

D. Comparison of measured results with predictions

In this section, we will compare the measured results with the prediction methodology discussed in Section III. We will examine each noise source individually and its physical mechanism of noise generation, then compare the overall noise level with the measured results. To do this, we have estimated aerodynamic quantities such as lift and drag coefficients, local incidence along the blade and wing span, boundary layer, etc., using XFOIL as discussed in a previous study [31]. Since the main aim of the research is to analyse the dominant noise mechanisms at various separation distances, we have utilised XFOIL to estimate approximate quantities that serve as inputs to the noise prediction models discussed in Section III. Predicting accurate aerodynamic quantities is beyond the scope of the current study and requires dedicated, in-depth investigation.

Figure 9a illustrates the comparison of measured and predicted overall noise levels with contributions from rearward potential field interaction and tonal wake-interaction. Here, rearward potential represents the noise due to unsteady load on the rearward propeller caused by the bound potential field of the upstream wing, while wake-interaction represents noise from the interaction of wing wakes with the downstream propeller. The results in Fig. 9a reveal that although there are considerable differences between measured and predicted results, the predictions follow the same trend as the measured results. This difference may arise from the numerous simplifications made in predicting aerodynamic quantities. More interestingly, we have plotted dominant contributions from viscous wake-interaction and potential field, allowing us to identify the regions dominated by individual mechanisms. The potential field turns out to be the dominant mechanism of noise generation at smaller separation distances and decreases rapidly with increasing separation distance between the rotor and wing. This is understandable because the wing has a strong bound potential field in its close proximity, which decreases rapidly as we move away. At lower separations, the propeller operates in the bound potential field of the wing, which produces unsteady loading on the propeller and acts as the dominant mechanism of noise generation. As we move further away from the wing, wake-interaction mechanism takes over and becomes the dominant mechanism. Since the strength of wake-interaction source does not decrease rapidly compared to the potential field, it continues to be a dominant mechanism over the range of separation distances considered in this study. To gain a clearer understanding, we have plotted the source strengths of both potential field and wake-interaction against measured noise levels, as shown in Figure 9b.

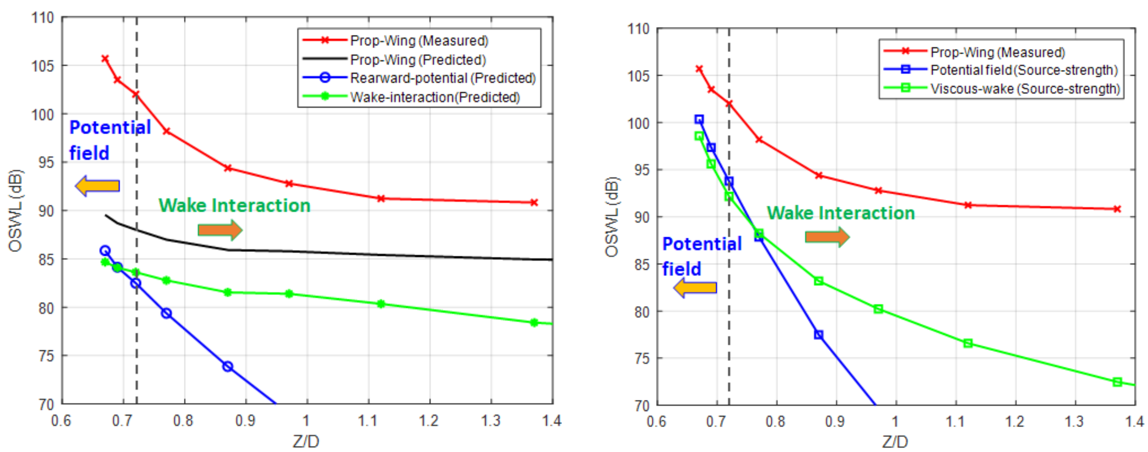

(a) Measured vs Predictions

(b) Source strengths of potential and wake interaction

Fig. 9 Comparison of measured and predicted noise over a range of separation distance in pusher configuration

It can be observed that at lower separation distances (approximately below $Z/D = 0.7$), the potential field has a higher source strength compared to wake-interaction, but it decreases rapidly with an increase in separation distance. Beyond $Z/D = 0.7$, wake interaction continues to be the dominant mechanism. The source strengths of the potential field and wake-interaction not only depend on the separation distance but also on the number of blades, flow speed, propeller rotational speed, etc. Therefore, changes in these parameters will alter this source balance and need to be considered while designing propeller-wing configuration for low-noise.

V. Conclusion

The results presented in this paper emphasize significant differences in noise signatures between an installed propeller in a pusher configuration and rotor-alone noise. When the propeller is placed near the wing, there's a noticeable shift in the noise generating mechanisms, resulting in different dominant sources of noise. The presence of airflow, simulating in-flight conditions, notably increases overall noise, encompassing both rotor-alone and interaction noise.

As the distance between the propeller and wing increases, the interaction decreases, leading to reduced unsteady loading on the propeller/wing system and a subsequent decrease in overall noise. This trend continues, with greater separation resulting in noise levels approaching those of rotor-alone noise. For the same thrust requirement and separation distance between the propeller and wing, the pusher configuration is found to be noisier than the puller configuration. Furthermore, this study offers a qualitative comparison of predicted noise levels with measurements, aiding in understanding dominant noise mechanisms at various propeller and wing separations. At low separation distances, the potential field is the dominant mechanism of noise generation, while at higher separations, wake-interaction sources become dominant. The strengths of these individual mechanisms depend on separation distance, flow speed, propeller rotational speed (thrust requirement), and the number of blades, among other factors, which alter this balance. Therefore, careful selection of these parameters is crucial in achieving a low-noise configuration when designing propeller-wing configurations.

Acknowledgments

This project has been funded by the Royal Academy of Engineering (RF\201819 \ 18 \ 194).The authors would like to acknowledge Rolls-Royce PLC for the financial and technical support through the Institute of Sound and Vibration Research at the University of Southampton. The authors would also like to thank Maxime Ethan Pennell and Owen Parnis for their help in running the experiments.

References

[1] Garrow, L. A., German, B. J., and Leonard, C. E., "Urban air mobility: A comprehensive review and comparative analysis with autonomous and electric ground transportation for informing future research," *Transportation Research Part C: Emerging Technologies*, Vol. 132, 2021, p. 103377.

[2] Mann, S., and Stuart, C., "Advanced propulsion through the 1990s-An airframer's view," *21st Joint propulsion conference*, 1985, p. 1192.

[3] Parry, A. B., "Theoretical prediction of counter-rotating propeller noise," Ph.D. thesis, University of Leeds, 1988.

[4] AIA, and Deloitte, "Aerospace Industries Association (AIA), Deloitte Study: US Advanced Air Mobility Market Could Reach $115B by 2035," , 2021.

[5] Ekoule, C. M., "Advanced open rotor far-field tone noise," Ph.D. thesis, University of Southampton, 2017.

[6] Blandeau, V., "Aerodynamic broadband noise from contra-rotating open rotors," Ph.D. thesis, University of Southampton, 2011.

[7] Akiwate, D. C., Parry, A., Joseph, P., and Paruchuri, C. C., "Analytical investigation of propeller-wing interaction noise," *28th AIAA/CEAS Aeroacoustics 2022 Conference*, 2022, p. 2877.

[8] Pagano, A., Barbarino, M., Casalino, D., and Federico, L., "Tonal and broadband noise calculations for aeroacoustic optimization of a pusher propeller," *Journal of Aircraft*, Vol. 47, No. 3, 2010, pp. 835–848.

[9] Griffith, E. D., and Revell, J. D., "Low Noise Propeller Technology Demonstration," Tech. rep., LOCKHEED-CALIFORNIA CO BURBANK, 1974.

[10] Akkermans, R. A., Pott-Pollenske, M., Buchholz, H., Delfs, J., and Almoneit, D., "Installation effects of a propeller mounted on a high-lift wing with a Coanda flap. Part I: aeroacoustic experiments," *20th AIAA/CEAS aeroacoustics conference*, 2014, p. 3191.

[11] Sinnige, T., "Aerodynamic and Aeroacoustic Interaction Effects for Tip-Mounted Propellers: An Experimental Study," Ph.D. thesis, Delft University of Technology, 2018.

[12] Zawodny, N. S., Boyd, D. D., and Nark, D. M., "Aerodynamic and Acoustic Interactions Associated with Inboard Propeller-Wing Configurations," *AIAA Scitech 2021 Forum*, 2021, p. 0714.

[13] Gutin, L., "On the sound field of a rotating propeller," *Physikalische Zeitschrit der Sowjetinion: Physical magazine of the Soviet Union volume 9 number 1*, Vol. 9, No. 1, 1948.

[14] Bradley, A. J., "A study of the rotor/rotor interaction tones from a contra-rotating propeller driven aircraft," *10th AIAA Aeroacoustics Conference, Seattle, WA, 8–11 Jul*, AIAA Paper 86-1894, 1986.

[15] Parry, A. B., and Crighton, D. G., "Prediction of counter rotation propeller noise," *12th AIAA Aeroacoustics Conference, San Antonio, TX*, Vol. AIAA Paper 1989-1141, 10-12 Apr, 1989.

[16] Hoff, G. E., "Experimental performance and acoustic investigation of modern, counter-rotating blade concepts," *NASA CR 185158*, 1990.

[17] Parry, A. B., “Modular prediction scheme for blade row interaction noise,” *Journal of Propulsion and Power*, Vol. 13, No. 3, 1997, pp. 334–341.

[18] Kingan, M. J., and Parry, A. B., “Acoustic theory of the many-bladed contra-rotating propeller: analysis of the effects of blade sweep on wake interaction noise,” *Journal of Fluid Mechanics*, Vol. 868, 2019, pp. 385–427.

[19] Kingan, M. J., and Parry, A. B., “Acoustic theory of the many-bladed contra-rotating propeller: effects of sweep on noise enhancement and reduction,” *Journal of Sound and Vibration*, Vol. 468, No. 115089, 2019b.

[20] Mukherjee, B., “A Preliminary Investigation of Propeller-Wing Interaction Noise for eVTOL Aircraft,” 2020.

[21] Boots, D. A., “Numerical Predictions of Propeller-Wing Interaction Induced Noise in Cruise and Off-Design Conditions,” Ph.D. thesis, Carleton University, 2016.

[22] Dierke, J., Akkermans, R. A., Delfs, J., and Ewert, R., “Installation effects of a propeller mounted on a wing with Coanda flap. Part II: numerical investigation and experimental validation,” *20th AIAA/CEAS aeroacoustics conference*, 2014, p. 3189.

[23] Akiwate, D. C., Parry, A. B., Joseph, P., and Paruchuri, C. C., “On the balance between the tonal and broadband noise of uninstalled propellers,” *AIAA AVIATION 2021 FORUM*, 2021, p. 2308.

[24] Amiet, R. K., “Noise due to turbulent flow past a trailing edge,” *Journal of Sound and Vibration*, Vol. 47, No. 3, 1976, pp. 387–393.

[25] Amiet, R., “Effect of the incident surface pressure field on noise due to turbulent flow past a trailing edge.” 1978.

[26] Roger, M., and Moreau, S., “Back-scattering correction and further extensions of Amiet’s trailing-edge noise model. Part 1: theory,” *Journal of Sound and vibration*, Vol. 286, No. 3, 2005, pp. 477–506.

[27] Rozenberg, Y., “Modélisation analytique du bruit aérodynamique à large bande des machines tournantes: utilisation de calculs moyennés de mécanique des fluides,” Ph.D. thesis, Ecole Centrale de Lyon, 2007.

[28] Drela, M., “XFOIL: An analysis and design system for low Reynolds number airfoils,” *Low Reynolds number aerodynamics*, Springer, 1989, pp. 1–12.

[29] Amiet, R. K., “Compressibility effects in unsteady thin-airfoil theory,” *AIAA Journal*, Vol. 12, No. 2, 1974, pp. 252–255.

[30] Amiet, R. K., “High frequency thin-airfoil theory for subsonic flow,” *AIAA journal*, Vol. 14, No. 8, 1976, pp. 1076–1082.

[31] Akiwate, D. C., and Parry, A., “Propeller wake interaction noise with downstream wing: effect of wing sweep, lean, and offset,” *AIAA AVIATION 2023 Forum*, 2023, p. 3357.